Microchimica Acta (2021) 188: 312
https://doi.org/10.1007/s00604-021-04977-w

ORIGINAL PAPER

Design of an amperometric glucose oxidase biosensor with added protective and adhesion layers

Rongwei Gao[1] · Xuelian Yang[1] · Qiuju Yang[1] · Yuanke Wu[1] · Feng Wang[2,3] · Qingyou Xia[2,3] · Shu-Juan Bao[1]

Received: 5 June 2021 / Accepted: 6 August 2021 / Published online: 29 August 2021

Abstract

Enzymes have demonstrated great potential in the development of advanced electroanalysis devices due to their unique recognition and catalytic properties. However, unsatisfactory stability and limited electron communication of traditional enzyme sensors seriously hinder their large-scale application. In this work, a simple and effective method is proposed to improve the stability of enzyme sensors by using sodium hyaluronate (SH) as a protective film, MXene-Ti_3C_2/Glucose oxidase (GOD) as the reaction layer, and chitosan (CS) /reduced graphene oxide (rGO) as the adhesion layer. Results demonstrate that the repeatability of the designed sensor increased by 73.3% after improving the adhesion between the reaction layer and the current collector and that its response ability was greatly enhanced. Moreover, the long-term stability of the electrode surface with SH protective film proved to be superior than that without protective film, which suggests that this design can effectively improve the overall performance of the enzyme biosensor. This work proposed a multi-tier synergistic approach for improving the reliability of enzyme sensors.

Keywords Enzyme sensor · Glucose determination · Nanomaterials · Electrochemistry · Protective film · Adhesion layer

Introduction

Electrochemical enzyme sensors have attracted tremendous attention due to their incomparable properties, such as specific selectivity, fast response, low cost, and easy miniaturization [1, 2]. Over the last decades, various electrochemical enzyme sensors have been reported, from simple test strips to wearable devices and implantable systems [3, 4]. Yet, only a few electrochemical enzyme sensors have practical application due to the instability and easy inactivation of enzyme [5]. It is well known that immobilized enzymes display higher activities and stabilities compared to free enzymes; thus, numerous works have focused on enzyme immobilization [6–10]. Specifically, a total of 8398 documents were retrieved from the Web of Science when searching the keyword "Enzyme immobilization" over the past 5 years. Although many enzyme sensors have been reported in the literature, only a few have been applied in various industries, such as blood glucose meters and pregnancy tests [11]. In addition to the effective immobilization of enzymes, other factors may restrict the practical application of enzyme sensors and, thus, require further investigation [9, 12].

Generally, enzyme sensors require a period of storage between preparation and use, which can affect their stability [13]. Enzyme contamination denaturation and loss of activity can also cause sensor failure. Since the test system is inseparable from the liquid for both intrusive and non-invasive sensors, poor enzyme immobilization can cause the enzyme to leach from the immobilized layer or the entire modified layer to peel off the electrode into the test solution, resulting in detection failure [3, 14]. On the other hand, the electrochemical sensing process generally includes enzymatic reactions and heterogeneous electron transfer reactions [15]. The key aims of this process are to achieve effective contact and accelerate the reaction kinetics between enzymes and detection molecules [16]. Thus, it is pertinent to maintain the enzyme

✉ Shu-Juan Bao
baoshj@swu.edu.cn

[1] Institute for Clean Energy and Advanced Materials, School of Materials and Energy, Southwest University, Chongqing 400715, People's Republic of China

[2] State Key Laboratory of Silkworm Genome Biology, Southwest University, Chongqing 400715, People's Republic of China

[3] Chongqing Engineering and Technology Research Center for Novel Silk Materials, Southwest University, Chongqing 400715, People's Republic of China

activity during the storage period, so that the active layer does not separate from the electrode surface under liquid operating conditions. The rapid realization and effective collection of the response signal of the enzyme toward target molecular are also highly important.

Herein, we propose an effective synergistic strategy to improve the stability and sensitivity of the enzyme sensor by combining the surface protective layer, intermediate reaction layer, and basic adhesion layer. As shown in Scheme 1, sodium hyaluronate (SH) is employed as the permeable protective film to protect enzymes from pollution and water loss, which is also beneficial to the diffusion of glucose toward the sensor's interface [17]. The reaction layer is constructed with MXene-Ti_3C_2/GOD, in which MXene-Ti_3C_2 can ensure the highly dispersed loading of GOD [18, 19]. The adhesion layer consists of CS/rGO, whereby the large specific area of rGO strengthens the bond between the modification layer and current collector, preventing the sensing surface from peeling off the collector during the test [20–23]. CS not only helps to bind MXene-Ti_3C_2 with rGO organically but also ensures high biocompatibility of the sensor. During the reaction, glucose passes quickly through the protective film (SH) into the reaction layer (MXene-Ti_3C_2/GOD) and reacts on the surface of GOD. Then, electrons are quickly released and effectively collected by the rGO-modified current collector. This method provides a new perspective for designing credible and stable enzymatic biosensor and expands its possible applications.

Experimental

All the chemical reagents were purchased and used without any further purification. Ti_3AlC_2 powders were purchased from Jilin 11 Technology Company Limited. Graphene oxide was purchased from Suzhou Tanfeng Graphene Technology Company Limited. And glucose oxidase (145,200 united/g) was purchased from Sigma-Aldrich Company Limited. Chitosan powders (analytical reagent (AR) grade), LiF (AR grade), and NaH_2PO_4 (AR grade) were purchased from Aladdin Industrial Corporation. Sodium hyaluronate (≥95 wt.% in H_2O) was purchased from Meilun Biotech Company Limited.

Synthesis Ti_3C_2Tx-MXene was obtained by etching layer A in MAX phase with LiF and HCl, which is reported by our previous work [30]. Graphene oxide (GO) was ultrasonically dispersed (1 mg/mL) in 0.1M NaH_2PO_4. Chitosan solution was obtained by adding 0.15g chitosan to 0.5 ωt% HAc solution.

Preparation of biochip Firstly, a layer of graphene oxide was electrodeposited on the electrode surface by cyclic voltammetry with a potential of −1.5 ~ 0.7 V. The scan was performed continuously for 15 cycles at a scan rate of 25 mV S^{-1}. The entire process was stirred and accompanied by Ar infusion. Secondly, one layer of chitosan was assembled on the surface of graphene by potentiostatic deposition with −2.5V deposition for 180 s, rinsing the electrode twice to remove dirt.

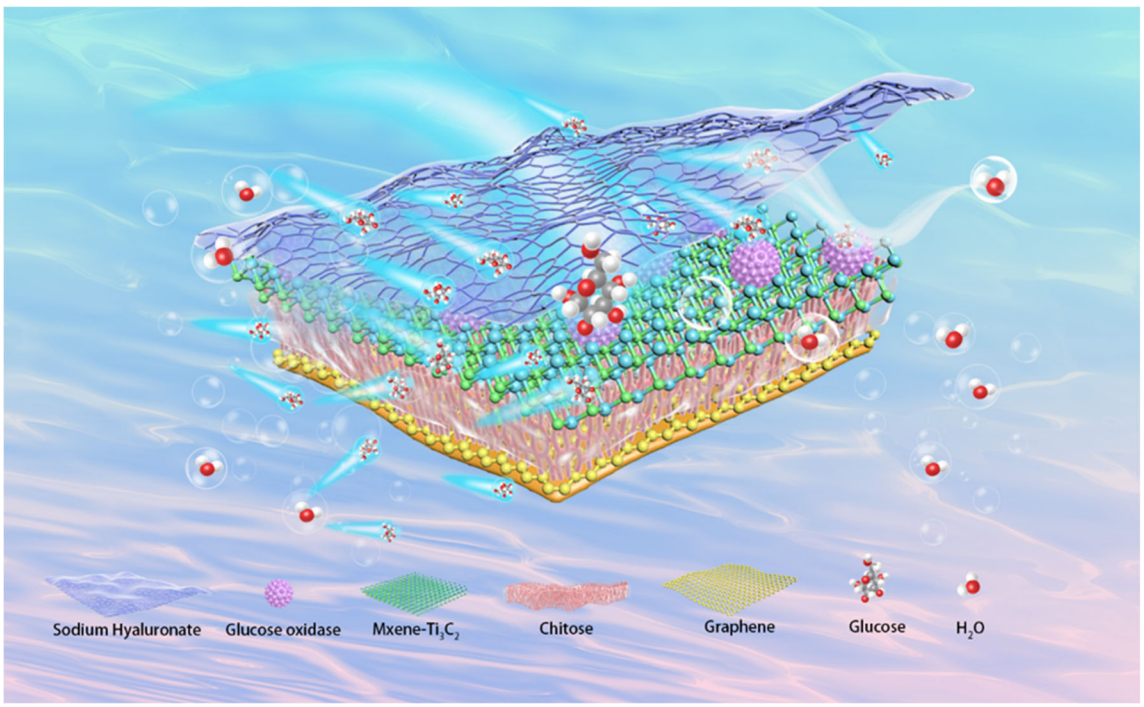

Scheme 1 Schematic illustration of the structure of the proposed glucose oxidase biosensor with added protective and adhesion layer

Finally, the glucose oxidase fixed MXene-Ti_3C_2 suspension was drip-coated on the electrode, and the modified material was fixed with 0.5% SH solution, and air-dried in a clean and closed environment. The prepared modified electrode should be stored in a refrigerator at 4 °C to maintain its biological activity. The enzyme activity units of our biosensor are 15.446 units/cm^2.

Electrochemical measurements The electrochemical workstation (CHI 660e, Shanghai, China) was used to evaluate the electrochemical performance of the biochip, in which a three-electrode system with the modified GCE, a platinum wire and a saturated Ag/AgCl electrode as the working electrode, the auxiliary electrode, and the reference electrode, respectively, was used. The PBS was deoxygenated by bubbling highly pure N_2 for at least 20 min and a N_2 atmosphere environment was kept in whole electrochemical measurements. For all electrochemical measurements, 0.01 mol L^{-1} PBS with pH 7.0 as electrolyte was used, and temperature was at 25 °C.

Serum samples preparation Human serum samples were obtained from three volunteers (about 5 μL), and dilute it 10 times by DI water. Then, mix tenfold dilution human serum samples (2.5 μL) into the air-saturated 0.01 mol L^{-1} pH 7.0 PBS (100 μL) solution as detection solution.

Material characterization Scanning electron microscope (FESEM, JSM-7800F) was used to observe the surface morphology of samples at 15 kv. EDS (INCA X-Max 250) data were collected to investigate the element distribution of samples. XRD diffraction pattern of samples was recorded by XRD-7000 (Shimadzu XRD-7000) powder X-ray diffraction. Nitrogen adsorption/desorption experiments were carried out at 77.3 K by means of quadrasorb evo 2QDS-MP-30 (Quantachrome Instruments) analyzer. The structure of materials was examined by Fourier transform infrared spectroscopy (FTIR, Tensor 207). The amount of GOD adsorption was determined by ultraviolet visible (UV-vis, UH4150, Hitachi High-Technologies Corporation) spectroscopy at 280 nm.

Results and discussion

Physical characterization of materials

MXene-Ti_3C_2 possesses the highest electromagnetic interference (EMI) shielding capability of all synthetic materials with similar thickness, good flexibility, easy processing, and high conductivity with minimal thickness. Meanwhile, MXene-Ti_3C_2 is also promising as antibacterial agents with higher efficiency than graphene oxide in diminishing bacterial cell viability [24–29]. Herein, the as-prepared MXene-Ti_3C_2 was explored as a new matrix to immobilize GOD in the fabricated biosensor for the ultrasensitive and rapid detection of glucose [30], which is illustrated in Fig. 1. XRD pattern in Fig. S1 confirms the perfect synthesis of MXene-Ti_3C_2, because the diffraction peak at around 6° is in accordance with the (002) lattice plane of MXene-Ti_3C_2. Figure S2 is the Raman spectrum of the MXene-Ti_3C_2, further verifying the successful synthesized. The FESEM images in Fig. 1a and b indicate that MXene-Ti_3C_2 possesses a graphene-like 2D nanostructure and has abundant folds and ultra-thin thickness. After loading GOD, energy-dispersive spectrometry (EDS) revealed that GOD was evenly dispersed on the surface of MXene-Ti_3C_2, as shown in Fig. 1c. The Barrett–Joyner–Halenda (BJH) pore-size distributions of the material before and after loading GOD are displayed in Fig. 1d; after loading GOD, the shape of the hysteresis loop changes and the specific area of the material decreases significantly, which due to lots of pores and folds of MXene-Ti_3C_2 were blocked by GOD absorbed on it. Furthermore, after loading GOD, the pore volume decreases (Table S1), which illustrates that GOD molecules have entered the inner pores of the MXene-Ti_3C_2. UV–vis spectroscopy was further performed to monitor the structural changes of GOD. Figure 1e (curve a) reveals the Soret absorption band of GOD immobilized in MXene-Ti_3C_2 at 450 nm, which is very close to that of native GOD (curve c). This indicates that GOD retained the essential features of its conformational integrity. IR spectroscopy can further examine the effectiveness of enzyme immobilization [31] (Fig. 1f). The peaks appeared at 683 and 643 cm^{-1}(Fig. 1f, curve c) for pure MXene-Ti_3C_2 correspond to the out-of-plane bending vibration of its O-H group, while the peaks centered at 1650 and 1544 cm^{-1} for pure GOD molecules ascribed to its typical amide I and amide II adsorption bands. After being adsorbed on porous MXene-Ti_3C_2, no obvious shift was observed for the characterized peaks of GOD, suggested that the activity of GOD was remained well (Fig. 1e, curve a). All the above results confirm that GOD was effectively immobilized on the surface of MXene-Ti_3C_2.

Electrochemical measurements

Cyclic voltammetry (CV) was employed to study the electrochemical activity of GOD on MXene-Ti_3C_2. CV of the porous MXene-Ti_3C_2/GOD-modified GCEs show a strong dependence on solution pH, as shown in Fig. S3. Stable and well-defined cyclic voltammograms can always be obtained in the pH range 5.18–9.06; the peak current increases with the increased pH until pH of 7.24, at which the current reaches the highest. Hence, further studies were focused on pH 7.24 PBS solutions. As shown in Fig. 2a, no obvious redox current can be seen in the CV curve of GOD/GCE, owing to the fact that redox centers of GOD are deeply packaged in the proteins. In contrast, well-defined redox peaks appeared at −348 mV and − 393 mV in the CV curve of MXene-Ti_3C_2/GOD/GCE,

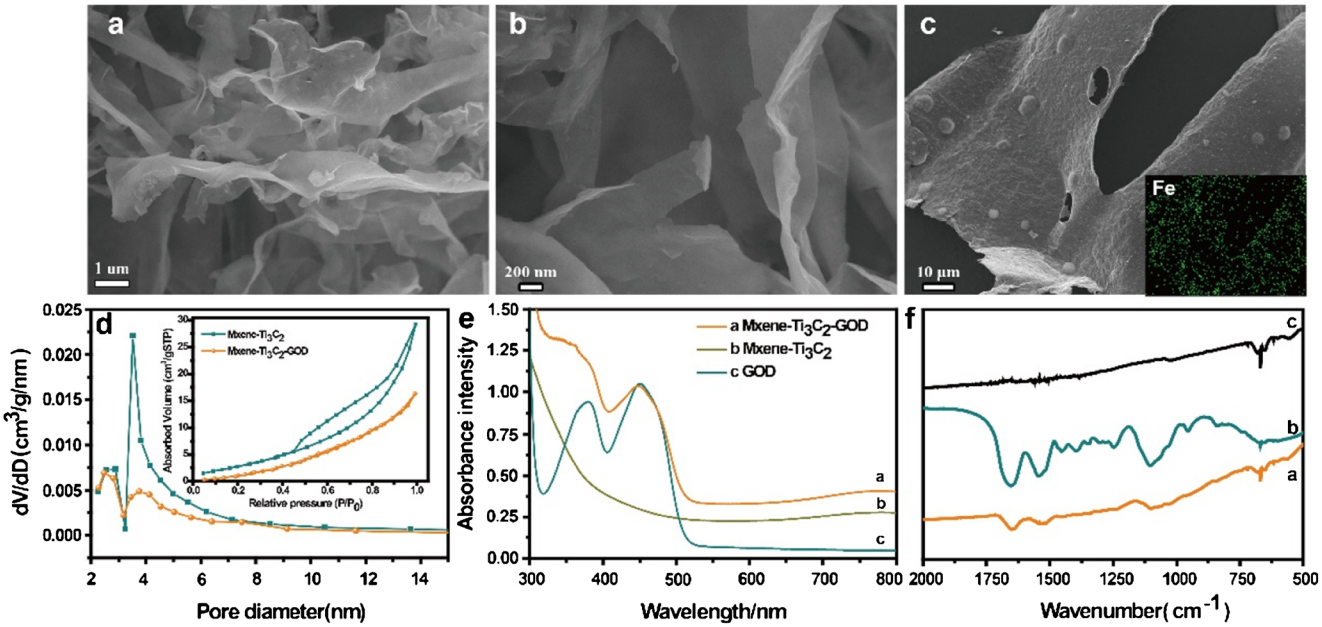

Fig. 1 **a** and **b** FESEM images of MXene-Ti_3C_2. **c** FESEM and EDS mapping (inset) of GOD-loaded MXene-Ti_3C_2. **d** BJH pore-size distributions of MXene-Ti_3C_2 before and after loading GOD and their corresponding nitrogen adsorption–desorption isotherms (inset). **e** UV-vis spectra of different samples. **f** FTIR of (a) GOD-loaded MXene-Ti_3C_2, (b) pure GOD, and (c) MXene-Ti_3C_2

which are consistent with the reported values for FAD/$FADH_2$ at pH 7.24. This finding suggests that MXene-Ti_3C_2 can effectively immobilize GOD to further realize direct electron transfer (DET). Furthermore, the effect of scan rate on the current response of MXene-Ti_3C_2/GOD/GCE is displayed in Fig. 2b. In 0.01M PBS, a pair of obvious reversible redox peaks can be observed, suggesting that the enzyme activity of GOD was remained well after embedding on the surface of MXene-Ti_3C_2. And both cathodic and anodic peak currents showed good linear relation with the increasing of scan rate from 20 to 200 mV s^{-1} (Fig. 2c), and correlation coefficients were determined to be 0.999 and 0.997, respectively, which suggested that the redox reaction of glucose on MXene-Ti_3C_2/GOD/GCE is a surface-controlled process [32,33]. Not only that, compared with rGO, MXene-Ti_3C_2 has a smaller specific surface area, so it has a smaller capacitance, which is conducive to improving the sensitivity of the sensor [32] (Fig. S4).

According to the results, the slack MXene-Ti_3C_2 sheets can effectively immobilize enzymes and help GOD achieve DET and respond well toward glucose. However, the repeatability of the performed experiment is disappointing (Fig. 3c). For instance, only 4 of the 15 MXene-Ti_3C_2/GOD/GCE electrodes we prepared under same conditions delivered clear and reversible redox peaks of GOD. This suggests that the effective fixation of nanomaterials does not guarantee that the natural enzyme maintains good electrochemical activity. A thorough literature review further revealed that CS is the most common biomaterial to improve the biocompatibility of composites [33–36]. Therefore, considering its good swelling property and viscosity, we used CS to modify electrode surface and then loaded MXene-Ti_3C_2/GOD. The subsequent results are promising, as displayed in Fig. 3f, whereby almost all electrodes delivered obvious redox peaks. This can be contributed to the appropriate biological microenvironment for

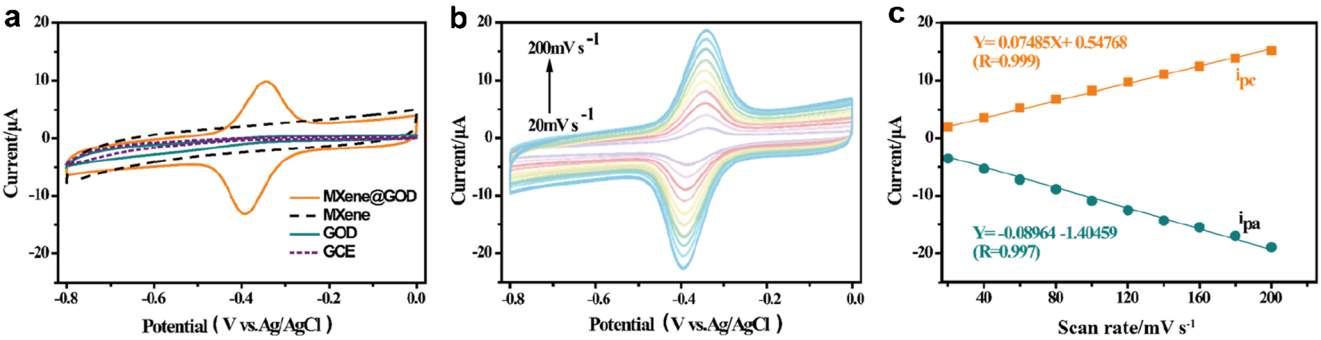

Fig. 2 **a** Cyclic voltammograms recorded at different modified GCE in 0.01 mol L^{-1} N_2-saturated PBS at 100 mV s^{-1}. **b** Cyclic voltammograms recorded at MXene-Ti_3C_2-GOD film electrode in 0.01 mol L^{-1} PBS at different scan rates (from 20 to 200 mV s^{-1}, inside to outside). **c** Plots of peak currents of MXene-Ti_3C_2-GOD film electrode versus scan rate.

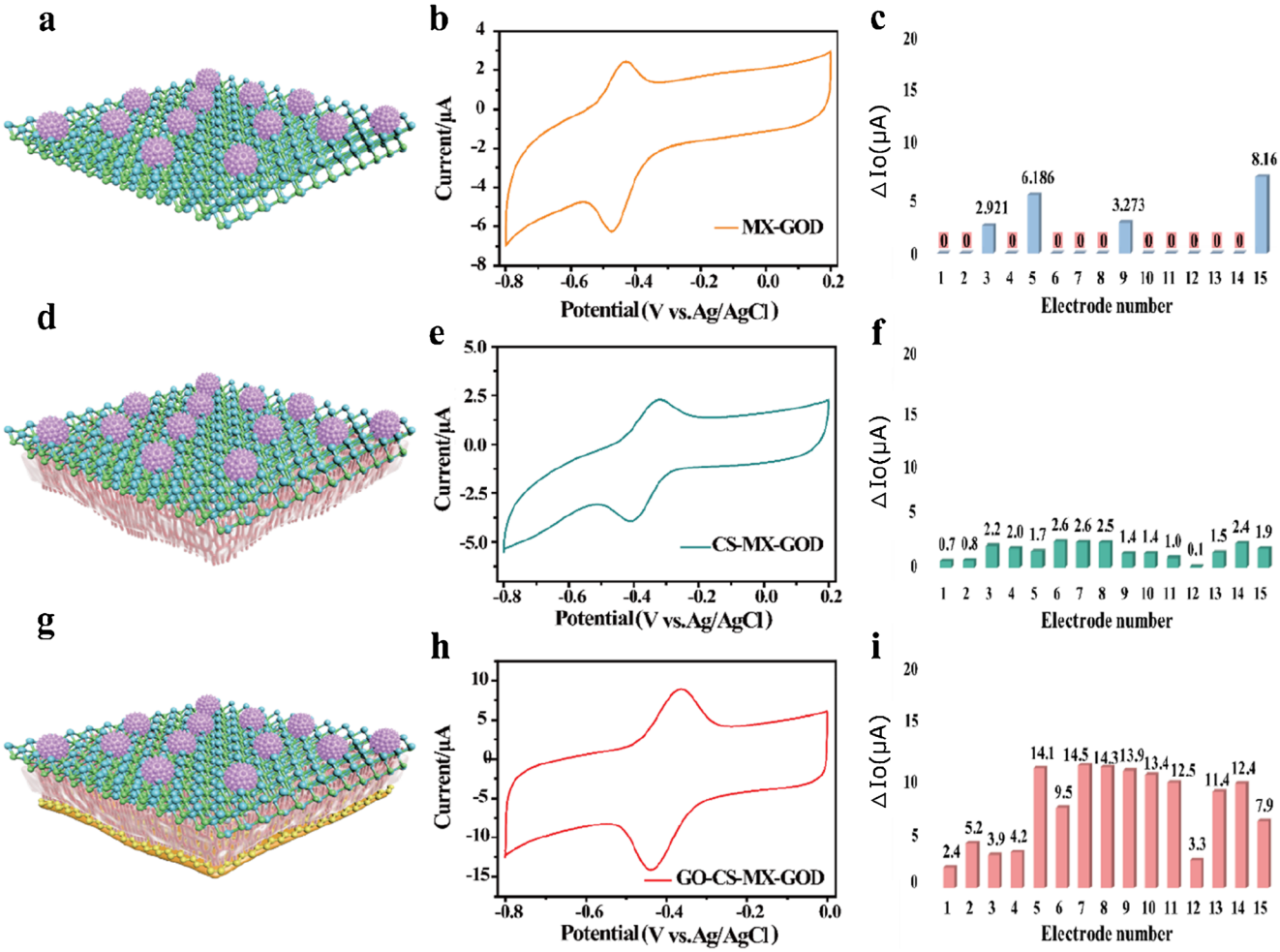

Fig. 3 Repeatability of various electrodes. **a** Schematic diagram of MXene-Ti_3C_2/GOD. **b** CV of MXene-Ti_3C_2/GOD in 0.01 mol L^{-1} N2-saturated PBS at 50 mV s^{-1}. **c** Bar chart of the CV peak current from 15 different MXene-Ti_3C_2/GOD/GCE. **d** Schematic diagram of CS/ MXene-Ti_3C_2/GOD. **e** Cyclic voltammograms recorded of CS/ MXene-Ti_3C_2/GOD in 0.01 mol L^{-1} N_2-saturated PBS at 50 mV s^{-1}. **f** Bar chart of the change value of the CV peak oxidation current at 15 different CS/ MXene-Ti_3C_2/GOD film electrodes. **g** Schematic diagram of rGO/CS/ MXene-Ti_3C_2/GOD. **h** Cyclic voltammograms recorded of rGO/CS/ MXene-Ti_3C_2/GOD in 0.01 mol L^{-1} N_2-saturated PBS at 50 mV s^{-1}. **i** Bar chart of the change value of the CV peak oxidation current at 15 different rGO/CS/MXene-Ti_3C_2/GOD film electrodes

GOD provided by CS. Although the repeatability of the electrodes steadily improved, Fig. 3e shows that the electrode performance was still not desirable. Particularly, the polarization of the electrode was more obvious due to the poor conductivity of CS, which may cause the insufficient transfer and collection of electrons.

Since the active layer fell off the electrode surface during the testing process, we then introduced the fixed rGO layer. As we all know, graphene possesses a large specific surface area and high electrical conductivity and, thus, has been widely applied in biosensor construction [37, 38]. In this work, we used rGO to modify the electrode, subsequently roughen the electrode surface, improve the adhesion of the electrode, and firmly increase bonding between the material and electrode. Meanwhile, the high electrical conductivity of rGO can enhance the electron transport performance. As shown in Fig. 3g-i, by introducing the rGO/CS/MXene-Ti_3C_2/GOD-modified electrode, a pair of obvious and symmetrical quasi-reversible redox peaks was observed. Under the same conditions, the peak current increased, indicating good reversible reaction characteristics. The experimental results further demonstrate that the repeatability of our designed sensor increased by 73.3% and that the response ability was also greatly improved. These enhancements may be attributed to the large surface of rGO, which can increase the roughness of the electrode surface without decreasing conductivity, so that stronger material fixation to the sensor is achieved and overall stability is improved. We also studied the electrochemical performance of the modified electrode using rGO/CS/rGO/GOD. In addition, the repeatability of different electrodes under the same conditions is shown in Table S2, and their standard deviations are less than 1.6. As shown in Fig. S5, compared to the rGO/

CS/MXene-Ti_3C_2/GOD electrode, the electrode with rGO immobilized enzyme has greater capacitance but a lower sensitivity, which is consistent with the result of comparing the capacitance of rGO and MXene-Ti_3C_2 above.

The long-term stability of the sensor is highly important for its use in practical applications [39]. In our experiment, we found that after modification with rGO/CS/MXene-Ti_3C_2/GOD, the stability of the fresh electrode in a single test was obviously improved. However, as the storage time increases, the sensor's performance still rapidly decayed (Fig. 4a). Obviously, the storage environment inevitably affects the sensor despite the strong fixation of GOD on MXene-Ti_3C_2. As a potential solution, we considered the introduction of a protective film to shield the sensor from the external environment and pollution without affecting the rapid penetration of the molecules to be detected. We were inspired by the sodium hyaluronate (SH) component of eye drops, which is a promising polymer material with excellent retention capacity (500 mL/g), network structure, and good biocompatibility, which is generally used to cover and protect articular cartilage and maintain the shape of cornea in eye tissues [17, 40]. Thus, a protective film composed of SH was employed to protect enzymes from pollution and water loss. As shown in Fig. 4d-f, after covering the GO/CS/MXene-Ti_3C_2/GOD/SH-modified electrode with the SH protective film, a higher peak current was achieved than that of GO/CS/MXene-Ti_3C_2/GOD, indicating a good reversible reaction characteristic. After 10 days of testing, the electrode remained active and achieved a desirable response current (ΔI) of 8.036 μA. This confirms that the active enzyme layer of the sensor requires a form of protection to maintain its long-term stability.

Biological samples detection

In order to investigate the practical application value of our designed sensor, it was employed to detect glucose concentrations in a simulation system and serum samples. As observed in Fig. 5a, due to the presence of the adhesion layer, the prepared GO/CS/MXene-Ti_3C_2/GOD/SH-modified film can tightly adhere to the electrode surface, which effectively solve the problem of material separation in the liquid environment to a certain extent. Figure 5b shows the typical current-time plot of the GO/CS/MXene-Ti_3C_2/GOD/SH electrode measured at −0.45 V by successive injections of glucose into the air-saturated and stirred 0.01 mol L^{-1} pH 7.0 PBS solution. The calibration plot (Fig. 5b inset) reveals the linear relationship between glucose concentration and sensor detection, where $Y = -0.93069 + 0.06868X$ and $R^2 = 0.999$, demonstrating a sensitivity of 98.1 μA mmol L^{-1} cm^{-2} and a linear response range of 39.8 μmol L^{-1} to 1.319 mmol L^{-1} and the limit of detection is 1.96 μmol L^{-1}. This represents a typical behavior of an enzymatic kinetic reaction [41]. Besides, it is observed that a fast response time of 4.0 s and each successive addition resulted in a decrease of the steady state current (Fig. 5c). To further verify feasibility, the GO/CS/MXene-Ti_3C_2/GOD/SH sensor was used to

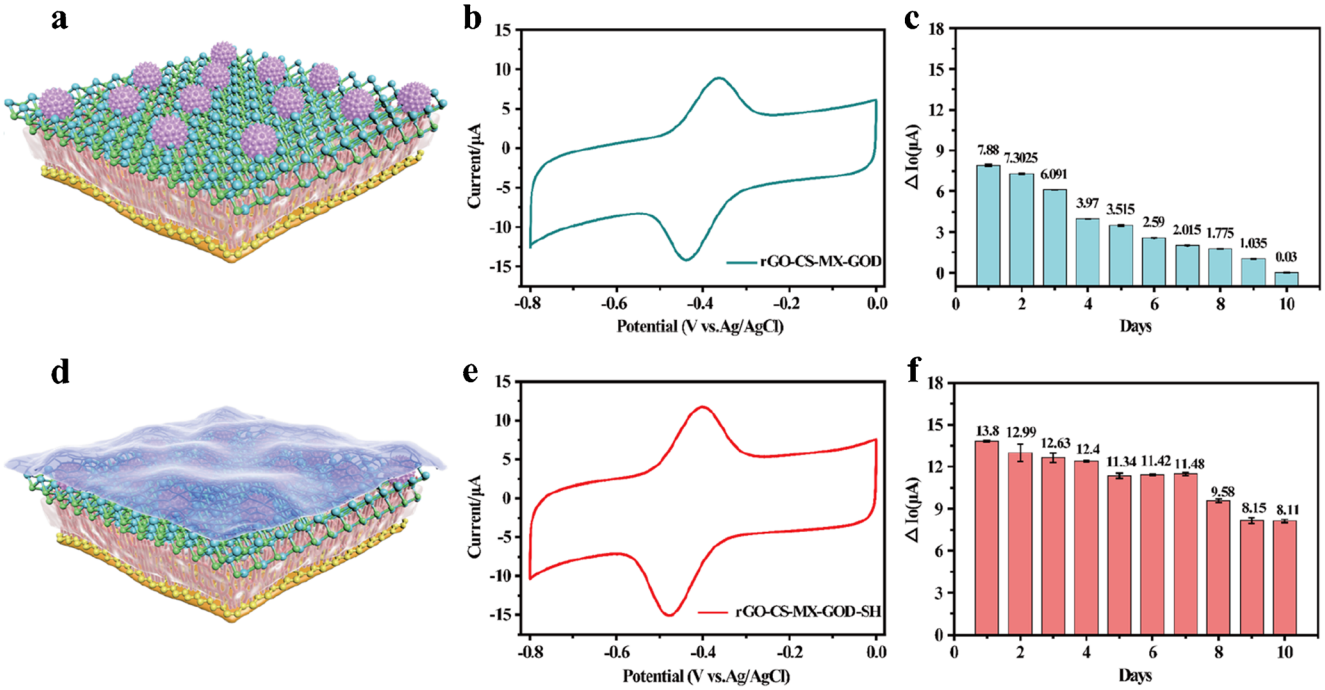

Fig. 4 Stability of various systems. **a** Schematic diagram of GO/CS/MXene-Ti_3C_2/GOD. **b** Cyclic voltammograms recorded of GO/CS/MXene-Ti_3C_2/GOD in 0.01 mol L^{-1} N_2-saturated PBS at 50 mVs^{-1}. **c** Ten-day stability of assembled GO/CS/ MXene-Ti_3C_2/GOD chip. **d** Schematic diagram of GO/CS/ MXene-Ti_3C_2/GOD/SH. **e** Cyclic voltammograms recorded of GO/CS/ MXene-Ti_3C_2/GOD/SH in 0.01 mol L^{-1} N_2-saturated PBS at 50 mVs^{-1}. **f** Ten-day stability of assembled GO/CS/MXene-Ti_3C_2/GOD/SH chip

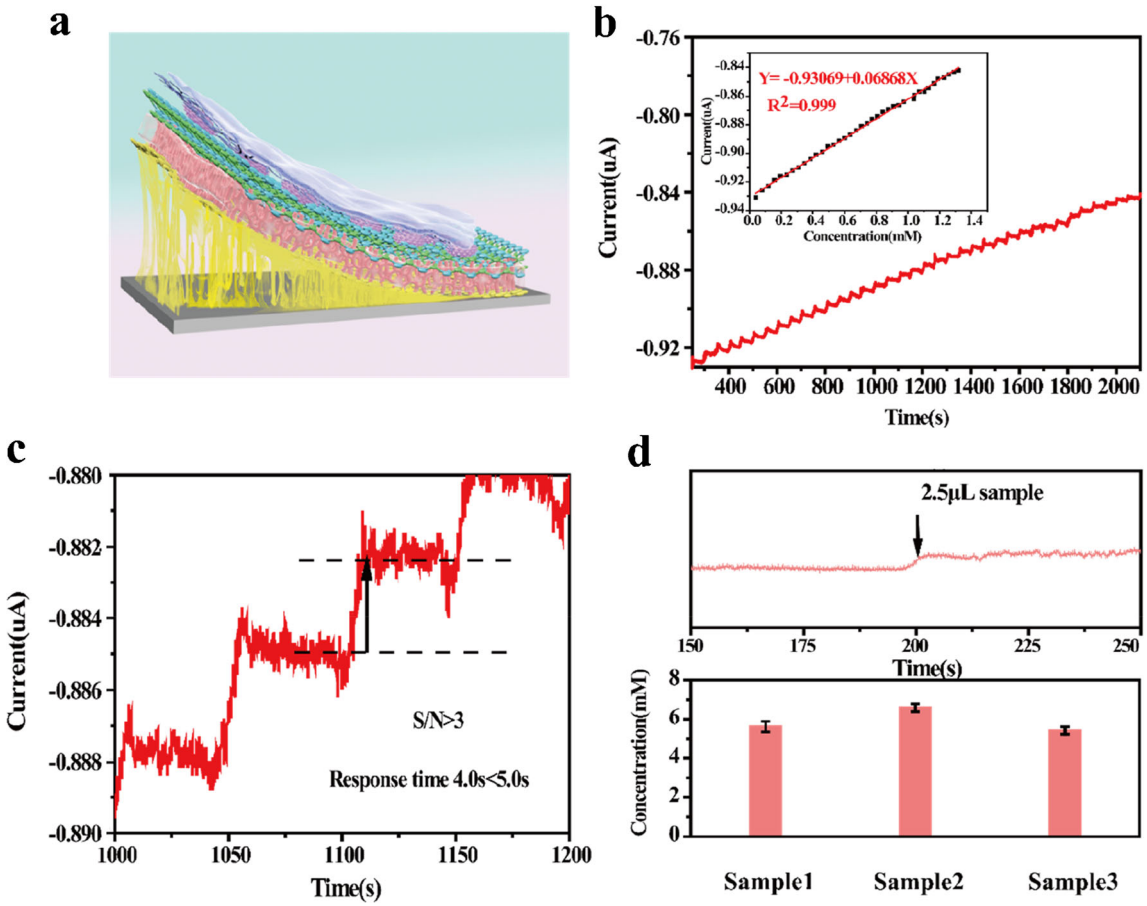

Fig. 5 **a** Schematic illustration of GO/CS/MXene-Ti_3C_2/GOD/SH hybrid film modified electrode. **b** Typical amperometric i-t curve for successive addition of different glucose concentrations of the sensor at −0.45 V. Insert of (**b**) shows the linearly relationship between current and glucose concentration and the response time after adding glucose. **c** Response time of the sensor. **d** The real sample testing.

detect glucose concentrations in serum samples, as shown in Fig. 5d. The results are summarized in Table S3, which demonstrate that the results are in good agreement with a commercial blood glucose test strip. Furthermore, the reported enzyme-based glucose sensors and their sensitivity, detection limit, and detection range are listed in Table S4; among of these results, the GO/CS/MXeneTi_3C_2/GOD/SH sensor shows the highest sensitivity, lower detection limit, and good linear range. Figure S6 further reveals its good selectivity for glucose in the present of various interferences (0.5 mmol L^{-1} AA, DA, UA, H_2O_2, KO_2, $NaHCO_3$, NaCl, and KCl). Overall, this method organically combines a protective layer, reaction layer, and adhesion layer to construct a highly active enzyme sensing interface by considering the excellent properties of the different layer materials. The results collectively demonstrate that the GO/CS/MXene-Ti_3C_2/GOD/SH sensor has huge potential in realizing practical applications of enzyme sensing.

Conclusion

In brief, this work proposes an effective method to improve the stability of enzyme sensors. The experimental results demonstrate that the stability of the developed enzyme sensor can be improved by combining multiple layers, including SH protective film, MXene-Ti_3C_2/GOD as the reaction layer, and CS/rGO as the adhesion layer. The practical and simple SH protective layer offers high biocompatibility and, thus, extends the potential applications of the enzymatic sensor. The nano-binding layer with graphene as the substrate, chitosan as the binder, and MXene-Ti_3C_2 immobilized enzyme as the active layer can effectively enhance the fixation between the active layer and electrode, improving electron transfer and collection. Conclusively, the proposed method provides a novel platform for designing other biosensors with excellent long-term stability and rapid detection, further expanding the practical applications of enzyme sensing.

Supplementary Information The online version contains supplementary material available at https://doi.org/10.1007/s00604-021-04977-w.

Funding We appreciate the support from the National Natural Science Foundation of China (no. 21972111, 21773188), Fundamental Research Funds for the Central Universities(XDJK2019AA002, XDJK2019B052), Natural Science Foundation of Chongqing (cstc2018jcyjAX0714), Chongqing Engineering Research Center for Micro-Nano Biomedical Materials and Devices, Chongqing Key Laboratory for Advanced

Materials and Technologies, and Venture and Innovation Support Program for Chongqing Overseas Returnees (cx2019073). We also thank Xuelian Yang, Qiuju Yang, and Yuanke Wu for helping with this work.

Compliance with ethical standards

Conflict of interest The authors declare that they have no competing of interests. This article does not contain any studies with human or animal subjects. Informed consent was obtained from all individual participants include in the study.

References

1. Lee H, Hong YJ, Baik S, Hyeon T, Kim DH, Glucose E-B, Lee H, Hong YJ, Baik S, Hyeon T, Kim DH (2018) Enzyme-Based Glucose Sensor: From Invasive to Wearable Device. Adv Healthc Mater 7:e1701150. https://doi.org/10.1002/adhm.201701150
2. Hao S, Zhang H, Sun X, Zhai J, Dong S (2020) A mediator-free self-powered glucose biosensor based on a hybrid glucose/MnO_2 enzymatic biofuel cell. Nano Res 14:707–714. https://doi.org/10.1007/s12274-020-3101-5
3. Bilal M, Iqbal HMN (2019) Chemical, physical, and biological coordination: an interplay between materials and enzymes as potential platforms for immobilization. Coord Chem Rev 388:1–23. https://doi.org/10.1016/j.ccr.2019.02.024
4. Garcia-Galan C, Berenguer-Murcia Á, Fernandez-Lafuente R, Rodrigues RC (2011) Potential of different enzyme immobilization strategies to improve enzyme performance. Adv Synth Catal 353:2885–2904. https://doi.org/10.1002/adsc.201100534
5. Liang T, Zou L, Guo X, Ma X, Zhang C, Zou Z, Zhang Y, Hu F, Lu Z, Tang K, Li CM (2019) Rising mesopores to realize direct electrochemistry of glucose oxidase toward highly sensitive detection of glucose. Adv Funct Mater 29:1903026. https://doi.org/10.1002/adfm.201903026
6. Piotr Mazurek PMZ, Skova AL (2020) Michael A Brook Enzyme Encapsulation in Glycerol–Silicone Membranes for Bioreactions and Biosensors. ACS Applied Polymer Materials 2:1203–1212. https://doi.org/10.1021/acsapm.9b01082
7. Seelajaroen H, Bakandritsos A, Otyepka M, Zboril R, Sariciftci NS (2020) Immobilized enzymes on graphene as nanobiocatalyst. ACS Appl Mater Interfaces 12:250–259. https://doi.org/10.1021/acsami.9b17777
8. Wu L, Wu S, Xu Z, Qiu Y, Li S, Xu H (2016) Modified nanoporous titanium dioxide as a novel carrier for enzyme immobilization. Biosens Bioelectron 80:59–66. https://doi.org/10.1016/j.bios.2016.01.045
9. Kienle DF, Falatach RM, Kaar JL, Schwartz DK (2018) Correlating structural and functional heterogeneity of immobilized enzymes. ACS Nano 12:8091–8103. https://doi.org/10.1021/acsnano.8b02956
10. Hwang ET, Lee S (2019) Multienzymatic cascade reactions via enzyme complex by immobilization. ACS Catal 9:4402–4425. https://doi.org/10.1021/acscatal.8b04921
11. Ozawa K, Iwasa H, Sasaki N, Kinoshita N, Hiratsuka A, Yokoyama K (2017) Identification and characterization of thermostable glucose dehydrogenases from thermophilic filamentous fungi. Appl Microbiol Biotechnol 101:173–183. https://doi.org/10.1007/s00253-016-7754-7
12. Cui H, Zhang L, Söder D, Tang X, Davari MD, Schwaneberg U (2021) Rapid and oriented immobilization of laccases on electrodes via a methionine-rich peptide. ACS Catal 11:2445–2453. https://doi.org/10.1021/acscatal.0c05490
13. Wu L, Lu Z, Ye J (2019) Enzyme-free glucose sensor based on layer-by-layer electrodeposition of multilayer films of multi-walled carbon nanotubes and Cu-based metal framework modified glassy carbon electrode. Biosens Bioelectron 135:45–49. https://doi.org/10.1016/j.bios.2019.03.064
14. Goh WJ, Makam VS, Hu J, Kang L, Zheng M, Yoong SL, Udalagama CN, Pastorin G (2012) Iron oxide filled magnetic carbon nanotube-enzyme conjugates for recycling of amyloglucosidase: toward useful applications in biofuel production process. Langmuir 28:16864–16873. https://doi.org/10.1021/la303046m
15. Li Y, Zhou J, Song J, Liang X, Zhang Z, Men D, Wang D, Zhang XE (2019) Chemical nature of electrochemical activation of carbon electrodes. Biosens Bioelectron 144:111534. https://doi.org/10.1016/j.bios.2019.111534
16. Weltz JS, Kienle DF, Schwartz DK, Kaar JL (2020) Reduced enzyme dynamics upon multipoint covalent immobilization leads to stability-activity trade-off. J Am Chem Soc 142:3463–3471. https://doi.org/10.1021/jacs.9b11707
17. Chiu YH, Chen MC, Wan SW (2018) Sodium hyaluronate/chitosan composite microneedles as a single-dose intradermal immunization system. Biomacromolecules 19:2278–2285. https://doi.org/10.1021/acs.biomac.8b00441
18. Gu H, Xing Y, Xiong P, Tang H, Li C, Chen S, Zeng R, Han K, Shi G (2019) Three-dimensional porous Ti_3C_2Tx MXene–graphene hybrid films for glucose biosensing. ACS Applied Nano Materials 2:6537–6545. https://doi.org/10.1021/acsanm.9b01465
19. Shao Y, Yao Y, Jiang C, Zhao F, Liu X, Ying Y, Ping J (2019) Two-dimensional MXene nanosheets (types Ti_3C_2Tx and Ti_2CTx) as new ion-to-electron transducers in solid-contact calcium ion-selective electrodes. Mikrochim Acta 186:750. https://doi.org/10.1007/s00604-019-3878-7
20. Santana ER, Spinelli A (2020) Electrode modified with graphene quantum dots supported in chitosan for electrochemical methods and non-linear deconvolution of spectra for spectrometric methods: approaches for simultaneous determination of triclosan and methylparaben. Mikrochim Acta 187:250. https://doi.org/10.1007/s00604-020-04225-7
21. Karaman C, Karaman O, Atar N, Yola ML (2021) Electrochemical immunosensor development based on core-shell high-crystalline graphitic carbon nitride@carbon dots and Cd0.5Zn0.5S/d-Ti_3C_2Tx MXene composite for heart-type fatty acid-binding protein detection. Mikrochim Acta 188:182. https://doi.org/10.1007/s00604-021-04838-6
22. Chen X, Qin P, Li J, Yang Z, Wen Z, Jian Z, Zhao J, Hu X, Jiao X (2014) Impedance immunosensor for bovine interleukin-4 using an electrode modified with reduced graphene oxide and chitosan. Microchim Acta 182:369–376. https://doi.org/10.1007/s00604-014-1331-5
23. Aslan S, Anik Ü (2015) Microbial glucose biosensors based on glassy carbon paste electrodes modified with Gluconobacter oxydans and graphene oxide or graphene-platinum hybrid nanoparticles. Microchim Acta 183:73–81. https://doi.org/10.1007/s00604-015-1590-9
24. Shahzad F, Alhabeb M, Hatter CB, Anasori B, Hong SM, Koo CM, Gogotsi Y (2016) Electromagnetic interference shielding with 2D transition metal carbides (MXenes). Science 353:1137–1140. https://doi.org/10.1126/science.aag2421
25. Wang B, Lai X, Li H, Jiang C, Gao J, Zeng X (2021) Multifunctional MXene/chitosan-coated cotton fabric for intelligent fire protection. ACS Appl Mater Interfaces 13:23020–23029. https://doi.org/10.1021/acsami.1c05222
26. Li L, Fu X, Chen S, Uzun S, Levitt AS, Shuck CE, Han W, Gogotsi Y (2020) Hydrophobic and stable MXene-polymer pressure sensors for wearable electronics. ACS Appl Mater Interfaces 12:15362–15369. https://doi.org/10.1021/acsami.0c00255

27. Gao Y, Liu G, Bu T, Liu Y, Qi Y, Xie Y, Xu S, Deng W, Yang W, Zhang C (2021) MXene based mechanically and electrically enhanced film for triboelectric nanogenerator. Nano Res. https://doi.org/10.1007/s12274-021-3437-5
28. Hu D, Wang S, Zhang C, Yi P, Jiang P, Huang X (2021) Ultrathin MXene-aramid nanofiber electromagnetic interference shielding films with tactile sensing ability withstanding harsh temperatures. Nano Res 14:2837–2845. https://doi.org/10.1007/s12274-021-3297-z
29. Neampet S, Ruecha N, Qin J, Wonsawat W, Chailapakul O, Rodthongkum N (2019) A nanocomposite prepared from platinum particles, polyaniline and a Ti_3C_2 MXene for amperometric sensing of hydrogen peroxide and lactate. Mikrochim Acta 186:752. https://doi.org/10.1007/s00604-019-3845-3
30. Yang Q, Yang T, Gao W, Qi Y, Guo B, Zhong W, Jiang J, Xu M (2020) An MXene-based aerogel with cobalt nanoparticles as an efficient sulfur host for room-temperature Na–S batteries. Inorganic Chemistry Frontiers 7:4396–4403. https://doi.org/10.1039/d0qi00939c
31. Bao S-J, Li CM, Zang J-F, Cui X-Q, Qiao Y, Guo J (2008) New nanostructured TiO2 for direct electrochemistry and glucose sensor applications. Adv Funct Mater 18:591–599. https://doi.org/10.1002/adfm.200700728
32. Singh E, Meyyappan M, Nalwa HS (2017) Flexible graphene-based wearable gas and chemical sensors. ACS Appl Mater Interfaces 9:34544–34586. https://doi.org/10.1021/acsami.7b07063
33. Samyn P (2021) A platform for functionalization of cellulose, chitin/chitosan, alginate with polydopamine: a review on fundamentals and technical applications. Int J Biol Macromol 178:71–93. https://doi.org/10.1016/j.ijbiomac.2021.02.091
34. Mohan K, Ganesan AR, Muralisankar T, Jayakumar R, Sathishkumar P, Uthayakumar V, Chandirasekar R, Revathi N (2020) Recent insights into the extraction, characterization, and bioactivities of chitin and chitosan from insects. Trends Food Sci Technol 105:17–42. https://doi.org/10.1016/j.tifs.2020.08.016
35. Tao F, Cheng Y, Shi X, Zheng H, Du Y, Xiang W, Deng H (2020) Applications of chitin and chitosan nanofibers in bone regenerative engineering. Carbohydr Polym 230:115658. https://doi.org/10.1016/j.carbpol.2019.115658
36. Jiang Z, Li N, Li PY, Liu B, Lai HJ, Jin T (2021) One-step preparation of chitosan-based magnetic adsorbent and its application to the adsorption of inorganic arsenic in water. Molecules 26. https://doi.org/10.3390/molecules26061785
37. Cai CJ, Xu MW, Bao SJ, Ji CC, Lu ZJ, Jia DZ (2013) A green and facile route for constructing flower-shaped TiO2 nanocrystals assembled on graphene oxide sheets for enhanced photocatalytic activity. Nanotechnology 24:275602. https://doi.org/10.1088/0957-4484/24/27/275602
38. Tan WC, Hofmann M, Hsieh Y-P, Lu ML, Chen YF (2012) A graphene-based surface plasmon sensor. Nano Res 5:695–702. https://doi.org/10.1007/s12274-012-0253-y
39. Babadi AA, Bagheri S, Hamid SB (2016) Progress on implantable biofuel cell: Nano-carbon functionalization for enzyme immobilization enhancement. Biosens Bioelectron 79:850–860. https://doi.org/10.1016/j.bios.2016.01.016
40. Kononova SV, Kruchinina EV, Petrova VA, Baklagina YG, Klechkovskaya VV, Orekhov AS, Vlasova EN, Popova EN, Gubanova GN, Skorik YA (2019) Pervaporation membranes of a simplex type with polyelectrolyte layers of chitosan and sodium hyaluronate. Carbohydr Polym 209:10–19. https://doi.org/10.1016/j.carbpol.2019.01.003
41. Lu S-Y, Lu Y, Jin M, Bao S-J, Li W-Y, Yu L (2017) Design and fabrication of highly sensitive and stable biochip for glucose biosensing. Appl Surf Sci 422:900–904. https://doi.org/10.1016/j.apsusc.2017.06.103